Comparative Study on the Performance of S-Shaped Diffuser With Shorten Length

Raed A. Jessam[1, 2], *Hussain H.* Al-Kayiem[2, *], and *Mohammad S.* Nasif[1]
[1]Mech. Eng. Dept., Universiti Teknologi PETRONAS, 32610 Bandar Seri Iskandar, Malaysia
[2]Electromechanical Eng. Dept., University of Technology, Baghdad, Iraq

Abstract. This study presents numerical investigation on the performance of S-shaped air intake normal and aggressive diffuser with 22% length reduction. Both models have same area ratio of 3.1 with different total length, turning angle and radius of curvature. The numerical investigation was implemented using CFD simulation by ANSYS-FLUENT 15 software. The inlet Reynold number was 4×10^4 and turbulence intensity 4.1%. The performance evaluation was performed throw evaluation the static pressure coefficient, pressure loss coefficient, distortion coefficient and static pressure wall coefficient. The numerical results show that the performance in the case of aggressive S-shaped diffuser has been reduced compared to the normal S-shaped diffuser. This reduction resulting from the early flow separation and increase of the separation zone due to the high curvature of top and bottom surfaces of aggressive S-shaped diffuser. The results show that the static pressure recovery coefficient decreased by 31%, the total pressure loss coefficient and distortion coefficient increased by 9.5% and 8.2%, respectively, compared to the S-shaped diffuser. The static pressure wall coefficient on the top and bottom surfaces was dropped with the aggressive S-shaped diffuser.

1 Introduction

In aero engines, the air intakes represent the main component of breathing of engine. The main function is to maintain high pressure recovery with less inflow to the engine. The performance of aero engines influenced by air intake so much. The S-shaped diffuser has a widely use compared to other types of intakes [1]. Therefore, the study of S-shaped diffuser one of the prevailing research subjects in mechanical engineering because of the important applications for example of aero engines. The size and weight constraints encourage to use shorter S-shaped diffuser. This process lead to aggressive S-shaped diffuser geometry with high diffusion. The ability to shorten the duct is possible by reducing the length but the risk of separation is going up and static pressure losses increase. S-shaped diffusers have increased cross-sectional areas and centerline curvatures with the flow direction. Secondary flows will be increase and cross-stream pressure gradients build up due to centerline curvature. The S-shaped diffuser must be achieving minimal total pressure losses and

* Corresponding author : hussain_kayiem@utp.edu.myg

facilitate almost uniform flow with small cross-flow velocity components at the outlet plane to be acceptable [2]. Maren et al [3] applied a new concept to reduce the length of S-duct, called integrated concept (IC), and compared with a base design. This concept represented by replacing the first row of low profile vane from the first bearing engine rotor by struts. The results show that total pressure loss base design is 4.4% and the total pressure loss with IC is 4.3%.

Other technique has been used by [4] to investigate numerically the effect of employing the energy promoters with different configurations on improving the performance of S-shaped aggressive diffuser. The results show that the static pressure recovery was improved by 47% and total loss coefficient was reduced by 56%. In the same way, LPVGs at first bend S-shaped have been investigated to study the influence of applying passive flow control on the flow separation [5]. Experimental study on the counter-rotating and co-rotating VGs configurations has been employed on the casing of aggressive interturbine S-duct [6]. The results show that the co-rotating VGs configurations were more active.

The objective of the present study is to investigate the effect of reduce the total length, thereby size reduction, on the performance of annular air intake S-shaped diffuser. The investigation was carried out on both normal and aggressive S-shaped diffusers numerically by CFD three-dimensional 3D simulations utilizing ANSYS-FLUENT 15 software. Static pressure recovery coefficient C_{PR}, total pressure loss coefficient C_{TL}, static pressure wall coefficient C_{WPR} and distortion coefficient $DC(45^o)$ have been adopted as indicators to compare the performance of both diffusers.

2 Proposed geometry

Figure 1 shows the proposed geometry of the investigated S-shaped diffuser. The modelled diffusers have area conduit for smooth air inflow with 65 mm long (b_i) × 65 mm height (l_i) and 65 mm long (b_o) × 125 mm height (l_i) at the outlet. The proposed geometry of the both models is only 45° section of the 360° of the complete annular shape of the diffuser. All the geometrical parameters for both models are summarized in Table 1

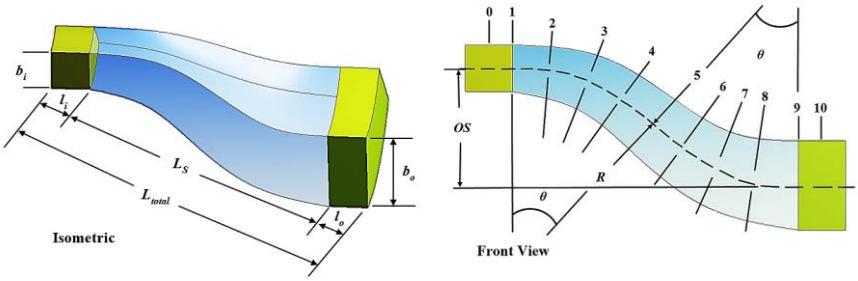

Fig. 1. Geometry of modeled S-shaped diffuser with interesting planes.

Table 1. Geometry specifications of S-shaped diffuser and S-shaped aggressive diffuser models.

Parameter	S-shaped diffuser	S-shaped aggressive diffuser
Area ratio, *AR (Ao/Ai)*	3.1	3.1
Model total length, L_{total}	526 mm	410 mm
Test section length, L_S	396 mm	280 mm
Turning angle, θ_b	45°/45°	35.3°/35.3°
Centreline turning radius, *R*	280 mm	242.5 mm

3 Performance indicators

The important indicators are using for performance evaluation of S-shaped diffuser are:

3.1 Static pressure recovery coefficient CPR

It represents the value of kinetic energy that has been converted into pressure energy due to diffusing at any position along the S-shaped diffuser, it can by denoted by the equation:

$$C_{PR} = \frac{P_s - P_{si}}{\frac{1}{2}\rho U_{av\,i}^2} \quad (1)$$

Where: P_s = static pressure (N/m^2), P_{si} = inlet static pressure (N/m^2) and $U_{av\,i}$ = average inlet velocity (m/s).

3.2 Total pressure loss coefficient C_{TL}

This indicator represented the value of lost total pressure as a proportion of the mean inlet dynamic pressure due to viscous forces and turbulent mixing, it represented by:

$$C_{TL} = \frac{P_{ti} - P_t}{\frac{1}{2}\rho U_{av\,i}^2} \quad (2)$$

Where: P_{ti} = inlet total pressure (N/m^2) and P_t = total pressure (N/m^2).

3.3 Wall static pressure coefficient C_{WPR}

It is represented by the following equation:

$$C_{WPR} = \frac{P_{ws} - P_{wsi}}{\frac{1}{2}\rho U_{av\,i}^2} \quad (3)$$

Where: P_{ws} = wall static pressure (N/m^2) and P_{wsi} = inlet wall static pressure (N/m^2)

3.4 Distortion coefficient $DC(45^o)$

It is represented by the following equation:

$$DC(45^O) = \frac{P_{tmax} - P_{t\min o}}{P_{tav\,o}} \quad (4)$$

Where: P_{tmin} = minimum total pressure at the outlet plane (N/m^2), P_{tmax} = maximum total at outlet plane pressure (N/m^2) and $P_{tav\,o}$ = average total at the outlet plane pressure (N/m^2).

4 Numerical approach

4.1 Governing equations

The governing equations for continuity and momentum, as well as for steady, turbulent, 3D, and incompressible flows of air are as expressed as follows:

The continuity equation in Cartesian coordinates (x, y, z):

$$\frac{\partial u}{\partial x} + \frac{\partial v}{\partial y} + \frac{\partial w}{\partial z} = 0 \quad (5)$$

X- Momentum equation:

$$\rho\left(u\frac{\partial u}{\partial x}+v\frac{\partial u}{\partial y}+w\frac{\partial u}{\partial z}\right)=-\frac{\partial P}{\partial x}+\rho g_x+\mu\left(\frac{\partial^2 u}{\partial x^2}+\frac{\partial^2 u}{\partial y^2}+\frac{\partial^2 u}{\partial z^2}\right) \quad (6)$$

Y- Momentum equation:

$$\rho\left(u\frac{\partial v}{\partial x}+v\frac{\partial v}{\partial y}+w\frac{\partial v}{\partial z}\right)=-\frac{\partial P}{\partial y}+\rho g_y+\mu\left(\frac{\partial^2 v}{\partial x^2}+\frac{\partial^2 v}{\partial y^2}+\frac{\partial^2 v}{\partial z^2}\right) \quad (7)$$

Z- Momentum equation:

$$\rho\left(u\frac{\partial w}{\partial x}+v\frac{\partial w}{\partial y}+w\frac{\partial w}{\partial z}\right)=-\frac{\partial P}{\partial z}+\rho g_z+\mu\left(\frac{\partial^2 w}{\partial x^2}+\frac{\partial^2 w}{\partial y^2}+\frac{\partial^2 w}{\partial z^2}\right) \quad (8)$$

By solving the equations from (5) to (8) the flow field have been predicated. The 3D Standard *k–ε* turbulence model has been adopted for quantities simulation. Near-wall scheme is performed with enhanced wall treatment to address the boundary layer formed during grid generation.

4.2 Boundary conditions

The average inlet velocity, inlet pressure and outlet gauge pressure as listed in Table 2. Diffuser walls considered as no slip boundary condition and all simulation cases were performed with standard air at temperature 30° C.

Table 2. Description of boundary conditions.

No	Boundary conditions	Value	No	Boundary conditions	Value
1	Inlet velocity	9.4(m/s)	4	Wall shear condition	No-slip
2	Turbulence intensity	4.1%	6	Air Density(ρ)	1.165 kg/m^3
3	Pressure (outlet)	0 Pa	7	Air Viscosity(μ)	1.85×10^5 kg/ m.s

4.3 Mesh generation and mesh independence

The geometry of S-shaped diffuser has been modeled by modular design ANSYS 15 and generated by ANSYS - FLUENT 15. To determine the optimum number of mesh cells used to obtain accurate solution, a mesh refinement has been conducted. Mesh independence study based on the C_{WPR} to select the optimum number of elements as in Table 3.

Table 3. Static pressure wall coefficient C_{WPR} variation with refining the grid of S-shaped aggressive diffuser compared to the experimental case.

No. of elements	Static Pressure Wall Coefficient C_{WPR}					
	Top surface		Deviation	Bottom surface		Deviation
	Exp.	CFD		Exp.	CFD	
183402	0.759	0.931	23 %	0.795	0.958	21%
214417		0.893	18 %		0.926	16.5%
666976		0.856	13 %		0.901	13.3%
843827		0.825	9.2 %		0.864	9.5%

It is obvious with the finer mesh 843827 elements the results were very close with previous experiment case of 9.2% and 8.6% for the top and bottom surfaces, respectively. Therefore, 843827 elements are used as the optimum number of mesh for the simulation.

5 Results and discussion

The numerical results show that the C_{PR} has been reduced by 31%. This drop created from the high bending surface of diffuser which is accelerate the flow especially on the bottom surface, thereby increase the flow separation and reduce the static pressure of aggressive S-shaped diffuser. Also, the C_{TL} was increased by 9.5% with aggressive diffuser. Fig.2 explains the distribution of velocity vectors and contours at the outlet plane for both diffusers and it can observe higher velocity with aggressive diffuser and cover larger area Fig.2-A compared to S-shaped diffuser Fig.2-B. Also, strong counter-rotating vortices, with bounded circular area, on the corners of the bottom surface of aggressive S-shaped diffuser were generated. This process leading reduces C_{PR} and increase the C_{TL} at the outlet plane.

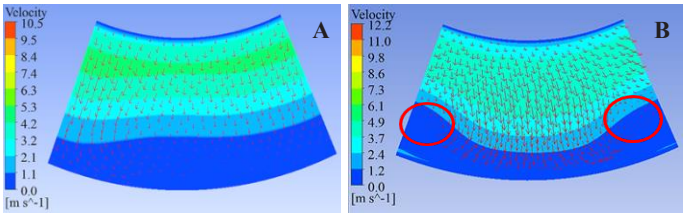

Fig. 2. Velocity vectors and velocity contours at the outlet plane of: A-normal S-shaped diffuser and B- aggressive S-shaped diffuser.

The other important indicator used for performance evaluation is *DC(45º)*. The total pressure values with measured data and numerical results of aggressive diffuser was higher, also, the difference between the maximum and minimum values was large compared with values of normal diffuser, as shown in Fig.3-A and 3-B. This large difference increases the *DC(45º)* at the outlet plane and reduces the flow uniformity at the outlet plane. The *DC(45º)* was increased by 8.2% of the aggressive diffuser compared to normal diffuser as explain in Table 4.

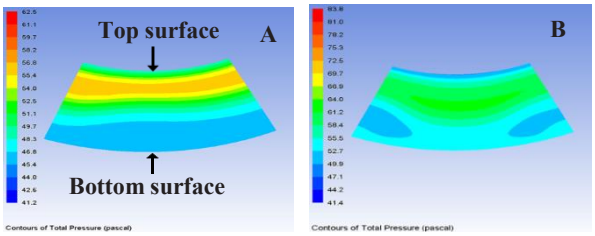

Fig. 3. Total pressure contours at the outlet plane of S-shaped diffuser: A. normal B. aggressive.

Table 4. Performance parameters of S-shaped diffuser and S-shaped aggressive diffuser models.

Performance Parameter	S-shaped diffuser	S-shaped aggressive diffuser
C_{PR}	0.76	0.58
C_{TL}	0.114	0.126
$DC\ (45)^o$	0.168	0.183

Fig. 4 shows the results of C_{WPR} along the length of the normal diffuser and aggressive diffuser. In both diffusers, the bottom surfaces have an accelerated flow resulting from high diffusion due to the strong curvature at the first bend. The process drops the C_{WPR} to minimum value. After this drop, the C_{WPR} recovered by the deceleration due to increase in the cross-sectional area. The reduction in C_{WPR} with aggressive S-shaped diffuser is less than -0.2

compared to normal S-shaped diffuser -0.17. Also, the flow separation started at $X \approx 66$ mm of aggressive diffuser and at $X \approx 135$ mm of normal diffuser. After this reduction, the C_{WPR} starts recover until the outlet. For the top surface, the C_{WPR} was increased in the initial phase 0.61 and 0.69 up to plane 3 around $X \approx 90$ mm and $X \approx 125$ mm for normal and aggressive diffuser, respectively. After that the C_{WPR} decreased by the accelerated flow until plane 7 at $X \approx 200$ mm and $X \approx 270$ mm for normal and aggressive diffusers, respectively, when the flow reattached again and then it increases steadily till the outlet plane.

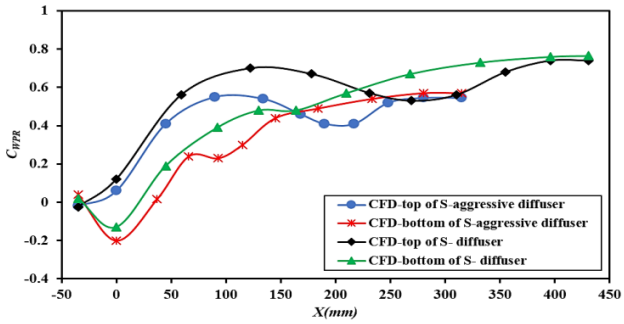

Fig. 4. Numerical Results of C_{WPR} along the length of normal S-shaped diffuser and aggressive S-shaped diffuser.

6 Conclusions

Numerical investigations have been conducted on normal S-shaped diffuser and aggressive S-shaped diffuser. The results indicated that reduction the total length of normal S-shaped diffuser to create a diffuser which has been named aggressive S-shaped diffuse resulting in a reduction in C_{PR} about 31%, increase the C_{TL} by 9.5% and $DC(45^o)$ by 8.2%. The flow separation was started early and the size of separation zone was large with aggressive S-shaped diffuser. This process leading to reduction in C_{WPR}.

The authors acknowledge Universiti Teknologi PETRONAS (UTP) - Malaysia for the logistic and technical support to produce this work. The first author appreciates UTP for the financial support to produce the paper under YUTP grant 0153AA-E61.

References

1. A. Madadi, M. J. Kermani, and M. Nili-Ahmadabadi. Journal of Engineering for Gas Turbines and Power **136**, no. 12, (2014).
2. Paul, A. R., Ranjan, P., Patel, V. K. and Jain, A. Aerospace Science and Technology **28**, no. 1, 332-343. (2013).
3. Marn, A., E. GÃķttlich, D. Cadrecha, and H. P. Pirker. Journal of turbomachinery **131**, no. 4, 041014, (2009).
4. R. A. Jessam, H.H. Al-Kayiem and M .S. Nasif, 2017. ARPN Journal of Engineering and Applied Sciences **12**, no. 7, (2017).
5. Santner, C., GÃķttlich, E., Marn, A., Hubinka, J. and Paradiso, B. Journal of Turbomachinery **134**, no.**1**, 011023. (2012).
6. Y. Zhang, S. Hu, X. F. Zhang, M. Benner, A. Mahallati, and Vlasic, E. Journal of Engineering for Gas Turbines and Power **136**, no. 11, 112604. (2014).